*Superlattices and Microstructures, Vol. 18, No. 3, 1995*

# Thermodynamic instability of Ag/Au and Cu/Pd metal superlattices

Z. W. Lu, B. M. Klein
*Department of Physics, University of California, Davis, California 95616, USA*

A. Zunger
*National Renewable Energy Laboratory, Golden, Colorado 80401, USA*

*(Received 19 July 1995)*

We show how the formation energies of $A_pB_q$ superlattices with arbitrary periods $p$ and $q$ and layer orientation $\hat{G}$ can be predicted via a 'cluster expansion' technique, given the formation energies of *short period* structures from first-principles calculations. We predict both bulk and epitaxial energies as well as the energies of the fully intermixed (alloyed) superlattices. Applications to Ag/Au and Cu/Pd superlattices illustrate our method, as well as a global classification scheme for superlattice stability.



## 1. Introduction

Advances in vaporization techniques have now led to the growth of metal-on-metal superlattices with quality approaching that of semiconductor superlattices. A central question regarding such superlattices (SL) is whether they are *thermodynamically* stable or that their post-growth stability is attributable to insurmountable kinetic barriers. This question can be phrased in terms of the superlattice excess enthalpy. We distinguish three types of pertinent excess enthalpies [1,2].

First, the *bulk formation enthalpy* $\Delta H_{SL}(pq,\hat{G})$ of the $A_pB_q$ superlattice with $p$ layers of $A$ atom followed by $q$ layers of $B$ atoms stacked in direction $\hat{G}$ (see a schematic diagram in Fig. 1) is the *equilibrium* superlattice energy (at lattice constant $a_{SL}$) minus that of equivalent amounts of constituents at their *bulk*, equilibria (at lattice constants $a_A$ and $a_B$, respectively):

$$\Delta H_{SL}(pq,\hat{G}) = E(A_pB_q,\hat{G},a_{SL}) - \left[\frac{p}{p+q}E_A(a_A) + \frac{q}{p+q}E_B(a_B)\right]. \quad (1)$$

This enthalpy represents the gain or loss of the superlattice energy with respect to the energy of bulk phase-separated constituents (so there is no interaction between the $A$ and $B$ atoms) and each of the constituents maintains its own (free-space) equilibrium structure.

Second, the *epitaxial formation enthalpy* $\delta H_{SL}$ $(pq, \hat{G}, a_s)$ is the energy of the superlattice grown coherently on a substrate with lattice constant $a_s$, relative to the energies of *epitaxial* constituents deformed to the same substrate $a_s$ and relaxed in the $\hat{G}$ direction:

0749-6036/95/070161 + 15 $12.00/0 

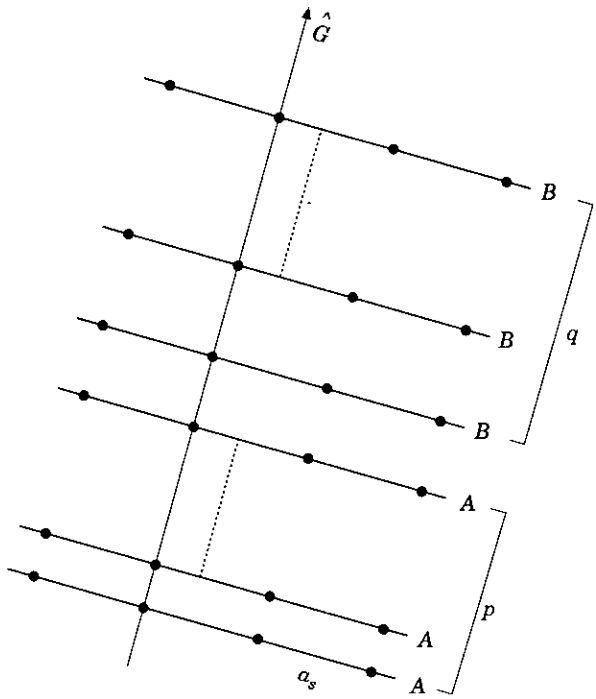


**Fig. 1.** Schematic diagam of an $A_pB_q$ coherent superlattice ($p$ layers of $A$ atoms followed by $q$ layers of $B$ atoms) along the $\hat{G}$ direction. $a_s$ is the substrate lattice constant perpendicular to $\hat{G}$.

$$\delta H_{SL}(pq,\hat{G},a_s) = E(A_pB_q,\hat{G},a_s) - \left[\frac{p}{p+q}E_A(\hat{G},a_s) + \frac{q}{p+q}E_B(\hat{G},a_s)\right]. \tag{2}$$

This enthalpy is pertinent to coherently strained interfaces where each component adopts the substrate dimension $a_s$ rather than its own equilibrium lattice constants $a_A$ and $a_B$. This coherency condition holds for films thinner than a critical thickness for misfit dislocations. For thicker films coherency is lost and eqn (1) replaces eqn (2).

Finally, the *mixing enthalpy of the disordered alloy* $\Delta H_{alloy}(x, T)$ is the energy of the random $A_{1-x}B_x$ alloy at the composition $x$ and equilibrium lattice constant $a(x)$ relative to equivalent amounts of constituents at their *bulk* equilibria

$$\Delta H_{alloy}(x,T) = E[A_{1-x}B_x, a(x)] - [(1-x)E_A(a_A) + xE_B(a_B)]. \tag{3}$$

These definitions suggest the following observations: (i) $\Delta H_{SL}(pq, \hat{G}) > 0$ reflects the propensity for *incoherent bulk decomposition* while $\Delta H_{SL}(pq, \hat{G}) < 0$ reflects the stability of the SL with respect to bulk decomposition. In contrast $\delta H_{SL}(pq, \hat{G}, a_s) > 0$ reflects the propensity for decomposition into *coherently matched constituents*. (ii) For substrate lattice constants matched to the equilibrium superlattice ($a_s = a_{SL}$) the difference

$$\Delta H_{SL}(pq,\hat{G}) - \delta H_{SL}(pq,\hat{G},a_{SL}) = \Delta E_{CS}(\hat{G}) \tag{4}$$

is the 'constituent strain' energy, i.e. the (orientiation dependent) energy required to deform the equilibrium free-space constituents ($A$ at $a_A$ and $B$ at $a_B$) into epitaxially strained constituents

$$\Delta E_{CS}(\hat{G}) = \frac{p}{p+q}[E_A(\hat{G}, a_s) - E_A(a_A)] + \frac{q}{p+q}[E_B(\hat{G}, a_s) - E_B(a_B)]. \quad (5)$$

For lattice matched constituents ($a_A \sim a_B$) we thus expect $\Delta E_{CS} \approx 0$ and $\delta H_{SL} = \Delta H_{SL}$ while in lattice mismatched systems $\Delta E_{CS} > 0$ and $\delta H_{SL} < \Delta H_{SL}$, so *bulk unstable SLs* ($\Delta H_{SL} > 0$) *can become epitaxially stable* ($\delta H_{SL} < 0$). Examples from semiconductor systems were discussed by Dandrea *et al.* [3] by Wood and Zunger [4] and by Zunger [2]. (iii) In the thick SL limit $p \to \infty$ and $q \to \infty$ the enthalpy per atom $\Delta H_{SL}$ has but a negligible $O(1/p)$ contribution from the $A/B$ interface. The remaining energy is that of the deformed constituents. Thus,

$$\Delta H_{SL}(pq \to \infty, \hat{G}) = \Delta E_{CS}(\hat{G}). \quad (6)$$

We thus define the 'interfacial energy' as the difference

$$\Delta H_{SL}(pq, \hat{G}) - \Delta H_{SL}(pq \to \infty, \hat{G}) = \delta H_{SL}(pq, \hat{G}, a_s) \equiv \frac{4I(pq, \hat{G})}{p+q}. \quad (7)$$

'Attractive interfaces' have $I < 0$ while 'repulsive interfaces' have $I > 0$. In most zinc blende semiconductors $I(210) < 0$ and $I(110) < 0$ are attractive interfaces $I(111) > 0$ is repulsive, while $I(100)$ can be either [3]. From eqns (6) and (7) we can write

$$\Delta H_{SL}(pq, \hat{G}) = \frac{4I(pq, \hat{G})}{p+q} + \Delta E_{CS}(\hat{G}). \quad (8)$$

Thus, the formation energy of the *bulk* superlattice consists of the interfacial term (which equals the *epitaxial formation enthalpy* in the absence of strain) and a constituent strain term. Figure 2 and Table 1 illustrate the various possibilities of the behavior of $\Delta H_{SL}$ versus $p$ in terms of the nature of the interfacial interactions ($I < 0$ or $I > 0$) and the existence/nonexistence of size mismatch between the constituents ($\Delta E_{CS} \approx 0$ or $\Delta E_{CS} > 0$). As the period $p$ increases, type I and II superlattices (both having $\Delta E_{CS} \approx 0$) approach zero enthalpy from above and from below, respectively, since they have $I > 0$ and $I < 0$, respectively. Type III and IV superlattices have finite enthalpy at long periods (due to frozen-in constituent strain).

(iv) While the signs of $\Delta H_{SL}$ and $\delta H_{SL}$ determine the stability towards phase-separation in bulk and in epitaxial forms, respectively, the stability towards intermixing (alloy formation) is decided by the 'ordering energy' $\Delta E_{ord}$. For bulk,

**Table 1:** This table illustrates type of superlattices according to 'constituent strain energy' $\Delta E_{CS}$ and 'interfacial energy' $I$.

| Type | Constituent strain energy | Interfacial energy | Example |
|---|---|---|---|
| Type I: | $\Delta E_{CS} \approx 0$ | $I > 0$ | Mo/W |
| Type II: | $\Delta E_{CS} \approx 0$ | $I < 0$ | Ag/Au |
| Type III: | $\Delta E_{CS} > 0$ | $I > 0$ | Pd/Rh |
| Type IV: | $\Delta E_{CS} > 0$ | $I < 0$ | Cu/Pd |

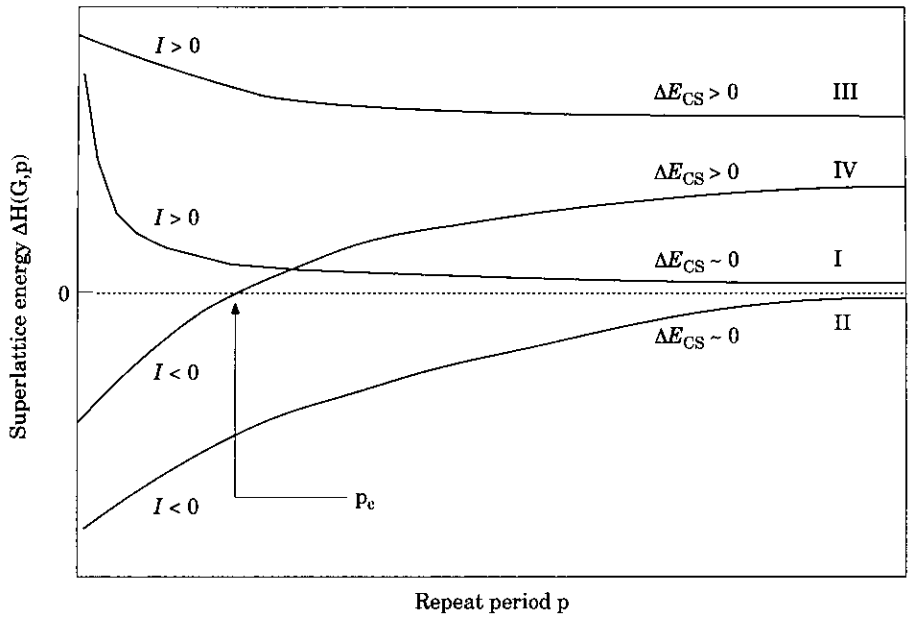


**Fig. 2.** Four prototypes of superlattice according to the sign of $\Delta H_{SL}$ and magnitude of $\Delta E_{CS}$. See definition in Table 1.

$$\delta E_{ord} = \Delta H_{SL}(pq, \hat{G}) - \Delta H_{alloy}(x, T) \tag{9}$$

where $x = q/(p+q)$ is the alloy composition, equivalent to that of a superlattice with period $A_pB_q$. If $\delta E_{ord} > 0$, the $A_pB_q$ superlattice will be stabilized by disordering into a bulk alloy, while if $\delta E_{ord} < 0$, the ordered SL is more stable at low temperature than the random alloy. Thus, for each of the types shown in Fig. 2 and Table 1, one can place the energy of the equivalent random alloy either below or above the ordered SL energy, resulting in sub-types 'a' and 'b', respectively. For example, lattice-mismatched superlattices with attractive interfaces (type IV) are stable for $p < p_c$ against phase separation (Fig. 2) but could be either stable [$\Delta H_{SL}(p < p_c) < \Delta H_{alloy}$] or unstable [$\Delta H_{SL}(p < p_c) > \Delta H_{alloy}$] towards intermixing.

While there were a few previous calculations on the stability of metal superlattices [5,6], they neglected the constituent strain effect or did not describe the general trends of stability versus period. Here we give a general framework for describing the thermodynamic stability of SLs and illustrate the method for two metal superlattices: Ag/Au and Cu/Pd. For relatively short periods $p$, it is possible to calculate $\Delta H_{SL}$ [eqn (1)] and $\delta H_{SL}$ [eqn (2)] directly from their definitions using, for example, first-principles LDA calculations. Such calculations become, however, rather time consuming as $p$ and the number of interesting orientations $\hat{G}$ increases. We describe here the 'cluster expansion' method that uses but a few, directly calculated $\Delta H_{SL}$ values (where we will also determine $a_{SL}$ and other internal and external structural parameters explicitly), mapping the result onto an Ising expansion so that $\Delta H$ can be evaluated trivially for *any* ($pq$, $\hat{G}$) (bypassing the determination of $a_{SL}$ and other structure-specific structural parameters). This Ising-like description has another advantage: once we know the interaction parameters of the CE, we can use standard methods of statistical mechanics, calculating the free-energy of any *given* SL as a function of temperature.

We find that Ag/Au SLs belong to type II (stable towards phase-separation at all periods [7]) while Cu/Pd is a type IV [stable towards phase-separation only for sufficiently short periods $p < p_c(\hat{G})$

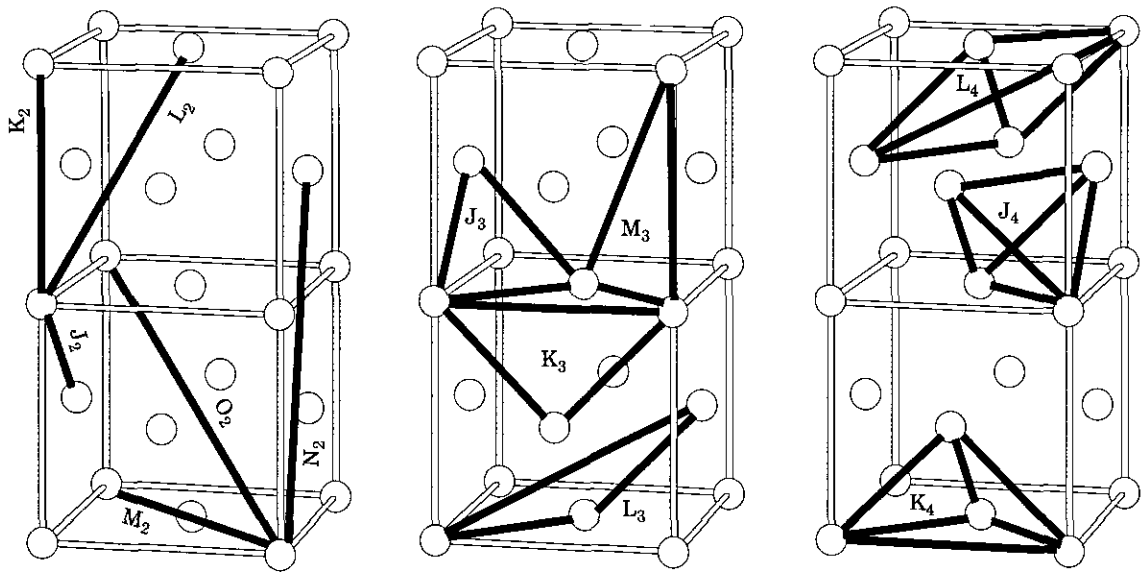


**Fig. 3.** Atomic figures used in the cluster expansion, which include pair figures, three-body figures, and four-body figures. See Table 4 for the definition of the figure coordinates.

that vary with orientation]. Regarding stability with respect to intermixing we find that both Ag/Au and Cu/Pd are stable towards alloying (sub-type 'a') only at short repeat periods $p_c = 1$–3: longer period superlattices, such as those actually grown, are predicted to be unstable at $T = 0$.

## 2. Method

Accurate first-principles total energy calculations (e.g. using the LDA) can be conveniently performed only on relatively short period superlattices [6]. For example, one can directly compute the total energy $\Delta H_{SL}(pq, \hat{G})$ of eqn (1) for a few ordered superlattice configurations denoted $\{\sigma_s\}$ with a reasonably small number of atoms in the unit cell. Our task here is to use a set of such directly calculated first-principles formation energies of simple ($s$) superlattices $\{\sigma_s\}$ to define a general 'cluster expansion' [1,8] that can predict the energies of all superlattices. In the CE, a superlattice made up of $A$ and $B$ atoms is treated as a lattice problem, assigning a set of 'spin' variables $\hat{S}_i$ ($i = 1, 2, \ldots, N$) to each of the $N$ sites of the lattice, with $\hat{S}_i = -1$ if site $i$ is occupied by an $A$ atom, and $\hat{S}_i = +1$ if it is occupied by a $B$ atom. A configuration $\sigma$ is then defined by the occupation of each of the $N$ lattice sites by an $A$ atom or a $B$ atom. The energies of any of the $2^N$ possible configurations $\sigma$ can be *exactly* [9] mapped into a generalized Ising Hamiltonian:

$$E(\sigma) = J_0 + \sum_i J_i \hat{S}_i(\sigma) + \sum_{j<i} J_{ij} \hat{S}_i(\sigma)\hat{S}_j(\sigma) + \sum_{k<j<i} J_{ijk} \hat{S}_i(\sigma)\hat{S}_j(\sigma)\hat{S}_k(\sigma) + \ldots, \tag{10}$$

where the $J$s are 'interaction energies', and the first summation is over all sites in the lattice, the second over all pairs of sites, the third over all triplets, and so on. The interaction energies $J$ are the same for all configurations $\sigma$. Thus, if the $J$s can be calculated and if the series [eqn (10)] converges reasonably rapidly, the energy $E(\sigma)$ of *any configuration* can be obtained almost immediately by simply calculating the spin products and summing eqn (10). The problem with representation (10) is

that often atoms move off their ideal lattice sites ('relaxation') and that when this happens the convergence of eqn (10) becomes slow [10–12]. This problem can be fixed [10]. To this end, the Ising series of eqn (10) is first cast in terms of lattice-averaged functions. The lattice is broken into a set of 'figures' $f$ (Fig. 3) each being a specific set of sites, such as a nearest-neighbor pair, or a nearest-neighbor triangle. Since the interaction energies have the full symmetry of the lattice, we can average the spin products of eqn (10) over each class $F$ of symmetry-equivalent 'figures'. This defines lattice-average spin-product for $F$

$$\bar{\Pi}_F(\sigma)=\frac{1}{ND_F}\sum_f \hat{S}_{i_1}(\sigma)\hat{S}_{i_2}(\sigma)\ldots\hat{S}_{i_m}(\sigma), \tag{11}$$

where $f$ run over the $ND_F$ figures in class $F$, and the spin indices run over the $m$ sites of figure $f$. In the remainder of this paper, we will use the term figure for a class of equivalent figures, as in 'the nearest-neighbor pair figure'. The set $\{\bar{\Pi}_F(\sigma)\}$ defines [9] a complete, orthogonal set of basis functions over the space defined by $\{\sigma\}$. This means that we can rigorously expand the energies of the configurations after all of the atoms have been fully relaxed—even though the atoms are no longer on their original lattice sites. We can therefore rewrite eqn (10) as a cluster expansion (CE):

$$\Delta E_{\mathrm{CE}}(\sigma)=N\sum_F D_F J_F \bar{\Pi}_F(\sigma) \tag{12}$$

We now take a few steps in anticipation of a possible slow convergence of eqn (12):

First, rather than expand $\Delta H_{\mathrm{SL}}(\sigma)\equiv\Delta E_{\mathrm{direct}}(\sigma)$, we will expand the energy with respect to a reference energy

$$\Delta E'_{\mathrm{CE}}(\sigma)=\Delta E_{\mathrm{direct}}(\sigma)-E_{\mathrm{ref}}(\sigma) \tag{13}$$

Second, we will separate the sum in eqn (12) into (i) a term including *all* pair interactions, which will be conveniently summed to infinity usig the reciprocal-space concentration-wave formalism, and (ii) the many-body terms which will be cast in real-space. This gives

$$\Delta E'_{\mathrm{CE}}(\sigma)=\mathbf{N}\sum_{\mathbf{k}} J(\mathbf{k})|S(\mathbf{k},\sigma)|^2+N\sum_F D_F J_F \bar{\Pi}_F(\sigma) \tag{14}$$

where the first term includes *all* pair interactions and the second term extends to $F$=many body figures. The Fourier transform of the real-space pair interaction $J_{0,n}$ between site 0 and site $n$ is

$$J(\mathbf{k})=\frac{1}{2}\sum_n^N J_{0,n}e^{i\mathbf{k}\cdot\mathbf{R}_n} \tag{15}$$

while the Fourier transform of the spin variables is

$$S(\mathbf{k},\sigma)=\frac{1}{N}\sum_l^N S_l(\sigma)e^{i\mathbf{k}\cdot\mathbf{R}_l} \tag{16}$$

where $\mathbf{R}_l$ (or $\mathbf{R}_n$) is the coordinate of the $l$th atomic site, and $\mathbf{k}$ is a vector in the first Brillouin Zone. For an ordered configuration $\sigma$, the $S(\mathbf{k},\sigma)$ functions will only be nonzero for a finite set of points $\mathbf{k}$.

Laks *et al.* [10] introduced, at this point, two modifications:

First, they required that $J(\mathbf{k})$ be a smooth function. This was accomplished by minimizing the integrated gradient of $J(\mathbf{k})$. Second, they selected $E_{\text{ref}}$ of eqn (13) to contain long range interaction terms so that the expansion of $\Delta E_{\text{direct}}(\sigma)-E_{\text{ref}}(\sigma)$ converges faster than otherwise. If relaxation is unimportant (e.g. Ag–Au) one might use $E_{\text{ref}}=0$. However, when relaxation is significant, there is a singular $\mathbf{k}=0$ term which can cause a slow decay of the real-space interactions, $J_{0,n}$ with distance $\mathbf{R}_0-\mathbf{R}_n$. In this case one can choose [10] $E_{\text{ref}}(\sigma)$ as the energy per atom of $p\to\infty$ superlattices $A_pB_p$ whose layers are oriented along the direction $\hat{G}(\sigma)$. This is the equilibrium 'constituent strain' [the *equilibrium value* of eqn (5)]. For each direction $\hat{G}$, some equilibrium (eq) value of $a_\perp$ will minimize this elastic energy $\Delta E_{\text{CS}}(\hat{G})$ yielding $\Delta E_{\text{CS}}^{\text{eq}}(\hat{G})$. One can compute $\Delta E_{\text{CS}}^{\text{eq}}(\hat{G})$ from its definitions by performing LDA calculations for epitaxially constrained $A$ and $B$ solids along directions $\hat{G}$, finding $a_\perp^{\text{eq}}$ at each $\hat{G}$. This 'direct' calculation, however, has to be repeated for all directions $\hat{G}(\sigma)$ for which a given lattice configuration $\sigma$ has $S(\mathbf{k},\sigma)\neq 0$. Laks *et al.* [10] has shown that this procedure can be simplified considerably if one assumes *harmonic* elasticity. In this case $a_\perp^{\text{eq}}(\hat{G})$ is computed analytically so the $\hat{G}$-dependence of $\Delta E_{\text{CS}}^{\text{eq}}(\hat{k}, x)$ is given in close-form. Details are given in Laks *et al.* [10].

The reference energy $E_{\text{ref}}(\sigma)$ which we subtract from $\Delta H_{\text{SL}}(\sigma)$ is hence

$$E_{\text{ref}}(\sigma)=N\sum_{\mathbf{k}} J_{\text{CS}}(\mathbf{k})|S(\mathbf{k},\sigma)|^2 \tag{17}$$

where

$$J_{\text{CS}}(\mathbf{k})=J_{\text{CS}}(\hat{k},x)=\frac{\Delta E_{\text{CS}}^{\text{eq}}(\hat{k},x)}{4x(1-x)}. \tag{18}$$

The reference energy of eqn (17) corresponds to an infinite series of *real-space* elastic interactions. Removing them from the relaxed LDA-calculated energies $\Delta H_{\text{SL}}(\sigma)$ prior to a cluster expansion significantly accelerates the convergence of this expansion [10].

Combing in a set $\{\Delta H_{\text{SL}}(\sigma_s)\}$ of LDA calculations on simple configurations $\{\sigma_s\}$ with eqns (13–18) we then fit $\Delta H_{\text{SL}}(\sigma_s)-E_{\text{ref}}(\sigma_s)$ to $\Delta E_{\text{CE}}(\sigma')$ of eqn (14). The reference energy is given by eqns (17–18). The input to our calculation are $N_a$ LDA formation energies $\{\Delta H_{\text{SL}}(\sigma)\}$ and the LDA epitaxial parameters needed to evaluate $\Delta E_{\text{CS}}^{\text{eq}}(\hat{G})$ of eqn (18). The output consists of the pair spectrum $J(\mathbf{k})$ (or, equivalently, its Fourier transform $J_{0,n}$), and the many-body interactions $\{J_F\}$. Together these enable calculations of the excess energy of *any* of the $2^N$ configurations $\sigma$ from

$$\Delta E_{\text{CE}}(\sigma)=N\sum_{\mathbf{k}}[J(\mathbf{k})+J_{\text{CS}}(\mathbf{k})]|S(\mathbf{k},\sigma)|^2+N\sum_{F} D_F J_F \bar{\Pi}_F(\sigma) \tag{19}$$

simply by inserting the geometrical factors $S(\mathbf{k}, \sigma)$ and $\bar{\Pi}_F(\sigma)$.

Convergence is tested by applying eqn (19) to a set of structures $\{\sigma'\}$ not used in constructing the CE fit. We define the prediction error (PE) as,

$$\delta_{\text{PE}}(\sigma')=E_{\text{direct}}(\sigma')-E_{\text{CE}}(\sigma'). \tag{20}$$

If the predictions errors are larger than a prescribed tolerance, more many-body figures and input structures are added to the expansion (14). This method has been tested [10] previously by comparing the prediction $\Delta E_{\text{CE}}(\sigma')$ to directly calculated energies of huge supercells (up to 1000 atoms) with

**Table 2:** Directly calculated relaxed LDA excess energies $\Delta E_{\text{direct}}(\sigma)$ (error $\pm 10$ meV atom$^{-1}$) and the corresponding cluster expanded [eqns (17) and (19)] formation energies $\Delta E_{\text{CE}}(\sigma)$ (in meV atom$^{-1}$) for Cu-Pd. Many structures calculated here can be characterized as a $Cu_pPd_q$ superlattice in orientation $\hat{G}$. We use the conventional structure (or prototype) name when available and assign our own label otherwise. Structure D1, D4, and D7 are defined in Figs 10 and 11 in Lu *et al.* [14]. The 'special quasirandom structures' (SQS) are structures with small number of atoms/cell used to mimic the random alloy. The structural information for these SQSs is given elsewhere [16–19]. The $L1_2$ based one-dimensional long period superlattices (LPS) are denoted by their Fisher and Selke (see [15]) notation which specifies, between angular brackets, the sequence of non anti-phased domains. The structures labeled here with the symbol * are used in the fit of eqn (19); others are predictions.

| Orientation formula | [001] | [011] | [012] | [111] |
|---|---|---|---|---|
| $AB$ | $L1_0$* | $L1_0$* | $L1_0$* | $L1_1$* |
| $\Delta E_{\text{direct}}$ | −86.3 | −86.3 | −86.3 | −82.0 |
| $\Delta E_{\text{CE}}$ | −82.2 | −82.2 | −82.2 | −81.0 |
| $A_2B$ | $\beta 1$* | $MoPt_2$ | $MoPt_2$ | $\alpha 1$* |
| $\Delta E_{\text{direct}}$ | −45.6 | −80.0 | −80.0 | −40.3 |
| $\Delta E_{\text{CE}}$ | −46.3 | −74.6 | −74.6 | −39.3 |
| $AB_2$ | $\beta 2$ | $MoPt_2$ | $MoPt_2$ | $\alpha 2$* |
| $\Delta E_{\text{direct}}$ | −72.0 | −45.7 | −45.7 | −49.2 |
| $\Delta E_{\text{CE}}$ | −65.6 | −54.6 | −54.6 | −49.8 |
| $A_3B$ | Z1* | Y1 | $DO_{22}$* | V1* |
| $\Delta E_{\text{direct}}$ | −32.9 | −65.9 | −76.4 | −20.0 |
| $\Delta E_{\text{CE}}$ | −41.0 | −56.4 | −77.8 | −22.2 |
| $AB_3$ | Z3* | Y3 | $DO_{22}$* | V3 |
| $\Delta E_{\text{direct}}$ | −50.2 | −36.6 | −46.4 | −34.1 |
| $\Delta E_{\text{CE}}$ | −59.2 | −47.5 | −47.0 | −34.4 |
| $A_2B_2$ | Z2* | Y2 | '40'* | V2 |
| $\Delta E_{\text{direct}}$ | −72.0 | −63.2 | −84.6 | −29.5 |
| $\Delta E_{\text{CE}}$ | −62.7 | −67.7 | −83.8 | −18.8 |
| Non-SL | $A$* | $B$* | $L1_2$ ($A_3B$)* | $L1_2$ ($AB_3$)* |
| $\Delta E_{\text{direct}}$ | 0.0 | 0.0 | −85.0 | −53.4 |
| $\Delta E_{\text{CE}}$ | 2.5 | 2.1 | −85.9 | −53.0 |
| Non-SL | $D1$ ($A_7B$) | $D7$ ($AB_7$) | $D4$ ($A_4B_4$)* | |
| $\Delta E_{\text{direct}}$ | −38.1 | −31.8 | −65.3 | |
| $\Delta E_{\text{CE}}$ | −30.7 | −24.9 | −65.5 | |
| | SQS8$_a$ ($A_4B_4$) | SQS8$_b$ ($A_4B_4$) | SQS14 ($A_6B_2$) | |
| $\Delta E_{\text{direct}}$ | −57.1 | −67.8 | −48.6 | |
| $\Delta E_{\text{CE}}$ | −54.5 | −69.7 | −43.6 | |
| | $DO_{23}$ ($A_6B_2$) | LPS⟨21⟩ ($A_9B_3$) | LPS⟨3⟩ ($A_9B_3$)* | LPS⟨4⟩ ($A_{12}B_4$) |
| $\Delta E_{\text{direct}}$ | −83.9 | −80.7 | −90.0 | −87.4 |
| $\Delta E_{\text{CE}}$ | −85.8 | −82.4 | −88.0 | −88.1 |

different symmetries (abrupt and inter-diffused superlattices, random alloys, impurities). The direct calculations as well as the corresponding CE were done using valence force field method [13]. Excellent agreement was found. Here we apply the method to find LDA energies of $(Ag)_p(Au)_q$ and $(Cu)_p(Pd)_q$ superlattices.

For Cu/Pd for which there is a significant size mismatch and hence relaxation, we use the full formalism of eqns (15–19). For Ag/Au for which the size mismatch is negligible we have $\Delta E_{\text{CS}} \approx 0$ so the cluster expansion is given by a finite real-space sum of both pair and many-body figures [eqn (12)].

**Table 3:** Directly calculated relaxed LDA excess energies $\Delta E_{direct}(\sigma)$ (error $\pm 2$ meV atom$^{-1}$) and the corresponding cluster expanded [Eq. (17) and (19)] formation energies $\Delta E_{CE}(\sigma)$ (in meV atom$^{-1}$) for Ag-Au. See caption for Table 2 for definition of the structures. The structures labeled here with the symbol * are used in the fit of eqn (19); others are for predictions.

| Orientation formula | [001] | [011] | [012] | [111] | [113] |
|---|---|---|---|---|---|
| $AB$ | $L1_0$* | $L1_0$* | $L1_0$* | $L1_1$* | $L1_1$* |
| $\Delta E_{direct}$ | −59.7 | −59.7 | −59.7 | −43.0 | −43.0 |
| $\Delta E_{CE}$ | −58.7 | −58.7 | −58.7 | −43.5 | −43.5 |
| $A_2B$ | $\beta 1$* | $MoPt_2$ | $MoPt_2$ | $\alpha 1$* | $MoPt_2$ |
| $\Delta E_{direct}$ | −40.8 | −49.7 | −49.7 | −30.2 | −49.7 |
| $\Delta E_{CE}$ | −40.4 | −47.2 | −47.2 | −29.0 | −47.2 |
| $AB_2$ | $\beta 2$ | $MoPt_2$ | $MoPt_2$ | $\alpha 2$* | $MoPt_2$ |
| $\Delta E_{direct}$ | −40.0 | −46.9 | −46.9 | −30.8 | −46.9 |
| $\Delta E_{CE}$ | −38.1 | −44.7 | −44.7 | −29.3 | −44.7 |
| $A_3B$ | Z1* | Y1 | $DO_{22}$* | V1* | W1 |
| $\Delta E_{direct}$ | −29.2 | −37.0 | −42.3 | −21.3 | −35.9 |
| $\Delta E_{CE}$ | −30.2 | −36.4 | −42.8 | −21.6 | −37.4 |
| $AB_3$ | Z3* | Y3 | $DO_{22}$* | V3 | W3 |
| $\Delta E_{direct}$ | −27.9 | −35.4 | −41.0 | −21.4 | −34.4 |
| $\Delta E_{CE}$ | −28.5 | −34.9 | −41.3 | −22.0 | −33.7 |
| $A_2B_2$ | Z2* | Y2 | '40'* | V2 | W2 |
| $\Delta E_{direct}$ | −28.8 | −44.1 | −55.3 | −22.9 | −50.6 |
| $\Delta E_{CE}$ | −29.5 | −42.0 | −54.9 | −21.9 | −49.4 |
| Non-Sl | Ag* | Au* | $L1_2$ ($A_3B$)* | $L1_2$ ($AB_3$)* | |
| $\Delta E_{direct}$ | 0.0 | 0.0 | −43.4 | −44.0 | |
| $\Delta E_{CE}$ | 0.3 | 0.1 | −43.5 | −44.3 | |
| Non-SL | D1 ($A_7B$) | D7 ($AB_7$) | D4 ($A_4B_4$)* | $SQS8_a$ ($A_4B_4$) | $SQS8_b$ ($A_4B_4$) |
| $\Delta E_{direct}$ | −20.8 | −20.0 | −42.9 | −42.5 | −43.6 |
| $\Delta E_{CE}$ | −23.0 | −20.5 | −43.6 | −42.2 | −42.4 |

## 3. Details of the calculations

### 3.1 Configurations used in fit

We used an input set which includes 18 structures for $Cu_{1-x}Pd_x$ covering compositions of $x=0$, 0.125, 0.25, 0.333, 0.5, 0.667, 0.75, 0.875, and 1 and orientations of [001], [011], [012], and [111]. Most of these can be viewed as short period $A_pB_q$ superlattices. These structures are $A$, $B$, $L1_0$, $L1_2$, $L1_2$, '40', $L1_1$, Z2, $DO_{22}$, $DO_{22}$, Z1, Z3, $a1$, $a2$, $\beta 1$, V1, D4 [14], and LPS $\langle 3 \rangle$ [15]. Tables 2 and 3 define these structures [14–19]. We included a few structures that are not superlattices, namely, the fcc $A$ and $B$, the $L1_2$, and the D4 structure. For Ag-Au [21], we used the same set (the structure LPS $\langle 3 \rangle$, which has more than 12 atoms cell$^{-1}$, was, however, not calculated).

### 3.2 Figures used in fit

For size-matched Ag-Au system, the pair-interactions are cast in real-space, i.e. $J_2$, $K_2$, $L_2$, and $M_2$ (up to fourth nearest neighbors), while for size-mismatched Cu-Pd system, the long-range pair-interactions are cast in reciprocal-space (up to $\sim 190$ neighbor shells). The many-body figures considered are given in Table 4. In addition to the nearest neighbor three ($J_3$) and four-body ($J_4$) interactions,

**Table 4:** Definition of the 'figures' $f$ used in our cluster expansion in terms of the vertices of the fcc structure (in units of $a/2$, where $a$ is the lattice parameter). We also give the interaction energies (meV atom$^{-1}$) for Cu-Pd and Ag-Au (see [18]). The pair interaction for Cu-Pd are cast in the reciprocal form. Here we also give the first-few pairs of real-space interaction energies. Negative (positive) $J_f$ denote ferromagnetic (antiferromagnetic) interactions.

| Cluster type | Designation | Vertices | Cu-Pd | Ag-Au |
|---|---|---|---|---|
| Empty | $J_0$ | | −100.41 | −42.53 |
| Point | $J_1$ | (000) | 14.66 | 2.59 |
| Pairs | $J_2$ | (000), (110) | 66.20 | 41.18 |
| | $K_2$ | (000), (200) | 8.26 | −0.18 |
| | $L_2$ | (000), (211) | 8.35 | 3.01 |
| | $M_2$ | (000), (220) | −0.25 | −1.22 |
| Triplets | $J_3$ | (000), (110), (101) | −26.87 | −0.06 |
| | $K_3$ | (000), (110), (200) | 8.37 | −3.05 |
| | $L_3$ | (000), (110), (211) | 6.16 | −0.40 |
| | $M_3$ | (000), (110), (002) | −2.50 | |
| Quadruplets | $J_4$ | (000), (110), (101), (011) | 6.26 | −0.03 |
| | $K_4$ | (000), (110), (101), (200) | −13.70 | |
| | $L_4$ | (000), (110), (101), (211) | −1.48 | |

we also included the following three and four body terms: $K_3$, $L_3$, $M_3$, $K_4$, and $L_4$, for Cu-Pd and $K_3$ and $L_3$ for Ag-Au.

### 3.3 Details of electronic structure calculations

We have calculated total energy versus volume $E(V)$ for the elemental fcc solids and compounds using the full-potential linearized augmented-plane-wave (LAPW) method [22–27], which is based on the local density approximation (LDA) [28].

For the Ag-Au systems, we have used the LDA exchange correlation potential of Ceperley and Alder [30], as parameterized by Perdew and Zunger [31]. To obtain highly precise results we use a **k**-point sampling scheme that is geometrically equivalent in the compound and its pure constituents [32]. For example, using such a set, the total energy of $A_3A$ in the $L1_2$ or $DO_{22}$ crystal structures are all equal to the fcc value. In practice we use sets of **k**-points that are equivalent to 408 fcc special **k**-points [33]: increasing the equivalent **k**-points from 60 to 408, the energy of each structure changes by less than 1 meV atom$^{-1}$, except for the Y1 and Y2 structures for which the changes are 1.2 and 1.6 meV atom$^{-1}$, respectively. We also use a large basis set cutoff of $R_{\mathrm{MT}}K_{\max}=9.0$ ($R_{\mathrm{MT}}^{\mathrm{Ag}}=R_{\mathrm{MT}}^{\mathrm{Au}}=2.55$ a.u.), which corresponds to $\sim$85 LAPWs atom$^{-1}$. The error in $\Delta E_{\mathrm{direct}}$ is estimated to be $\sim$2 meV atom$^{-1}$.

For the lattice mismatched Cu-Pd system, we also relax (assisted with quantum mechanically calculated forces) the symmetry-allowed degrees of freedom (both cell-internal and cell-external parameters). We have used the Wigner [34] form of exchange–correlation potential. The error in $\Delta E_{\mathrm{direct}}$ for Cu-Pd is however, larger than for Ag-Au, estimated to be $\sim$10 meV atom$^{-1}$. The calculated formation enthalpies for the ordered structures are given in Tables 2 and 3.

### 3.4 Examination of fitting errors

For Ag-Au, the average fitting error is 0.7 meV atom$^{-1}$ for 17 structures used to extract the interaction energies $\{J\}$. We have tested these interaction parameters by predicting $\Delta E_{\mathrm{direct}}$ for 15 struc-

tures $\{\sigma'\}$ that are not used to obtain $\{J\}$s. Comparing with directly-calculated LAPW values, we find an average prediction error of $\delta_{PE}=1.5$ meV atom$^{-1}$, with a maximum prediction error of 2.5 meV atom$^{-1}$. For Cu-Pd where a typical excess energy $\Delta E(\frac{1}{2})$ is around $-70$ meV atom$^{-1}$ we find an average fitting error of 3.9 meV atom$^{-1}$, an average prediction error of 6.2 meV atom$^{-1}$ (for 16 structures that are not used in the fit). Recall that the estimated LAPW convergence errors are 10 meV atom$^{-1}$ and 2 meV atom$^{-1}$ for Cu-Pd and Ag-Au, respectively.

## 4. Results

### 4.1 Interaction energies

Table 4 gives the values of many-body interaction energies for Ag-Au and Cu-Pd, while Fig. 4 shows the pair interaction energies for Ag-Ag and Cu-Pd. Note the dramatically different range for the relaxed Cu-Pd and unrelaxed Ag-Au systems since Ag and Au are nearly lattice-matched.

Table 5 gives the constituent strain energy $\Delta E_{CS}$ Cu-Pd at $x=\frac{1}{2}$ for $\hat{G}$ along the [001], [011], [012], and [111] directions. For size-matched Ag-Au systems $\Delta E_{CS}\approx 0$. This table also gives interfacial energies.

We find the following results:

(i) for long periods, the energy of Cu/Pd SLs is dictated by the constituent strain $\Delta E_{CS}$ while the energy of Ag/Au SLs is dictated by interfacial interactions $I$. The order of constituent strain energies in Table 5 (also the order of $\Delta H_{SL}$ for large $p$) is:

$$\Delta E_{CS}^{eq}(111)>\Delta E_{CS}^{eq}(011)>\Delta E_{CS}^{eq}(112)>\Delta E_{CS}^{eq}(001). \tag{21}$$

Thus, the (111) is the 'hardest' elastic direction while the (001) is the 'softest'. This is nearly universal results observed also in semiconductor superlattices [3]. We thus predict that for lattice mismatched *long* period SLs, the (001) oriented Cu-Pd SL is the least unstable while the (111) oriented SL is the most unstable.

(ii) Both Cu-Pd and Ag-Au have attractive ($I<0$) interfaces. The order of interfacial energies (Table 5) is

$$I(111)>I(001)>I(011)>I(012). \tag{22}$$

Thus, the (012) interface is the most stable, while the (111) interface is the least stable. Hence, in the absence of size-mismatch, the (012) oriented SL is the most stable and (111) oriented is the least stable.

(iii) Table 5 shows that Cu-Pd has considerably more attractive interfaces than Ag-Au. Since $\Delta E_{CS}\approx 0$ and $I<0$ for Ag-Au, this system behaves as Type 2 (Table 1). In contrast Cu-Pd $\Delta E_{CS}>0$ and $I<0$, so this is a type IV system. Thus, Ag/Au SLs are stable with respect to phase-separation at all periods $p$. Cu/Pd SLs are stable towards bulk phase-separation only if

$$\begin{aligned} p&<5 \text{ for } \hat{G}=(111)\\ p&<18 \text{ for } \hat{G}=(012)\\ p&<9 \text{ for } \hat{G}=(011)\\ p&<15 \text{ for } \hat{G}=(001). \end{aligned} \tag{23}$$

Above these values of $p$, the Cu/Pd bulk SLs are unstable with respect to phase-separation. Note that since $\delta H_{SL}(pp,\ \hat{G},\ a_s)=2I(pp,\ \hat{G})/p$ is *negative*, these systems will be stable against epitaxial phase-separation as long as interfacial coherence exists.

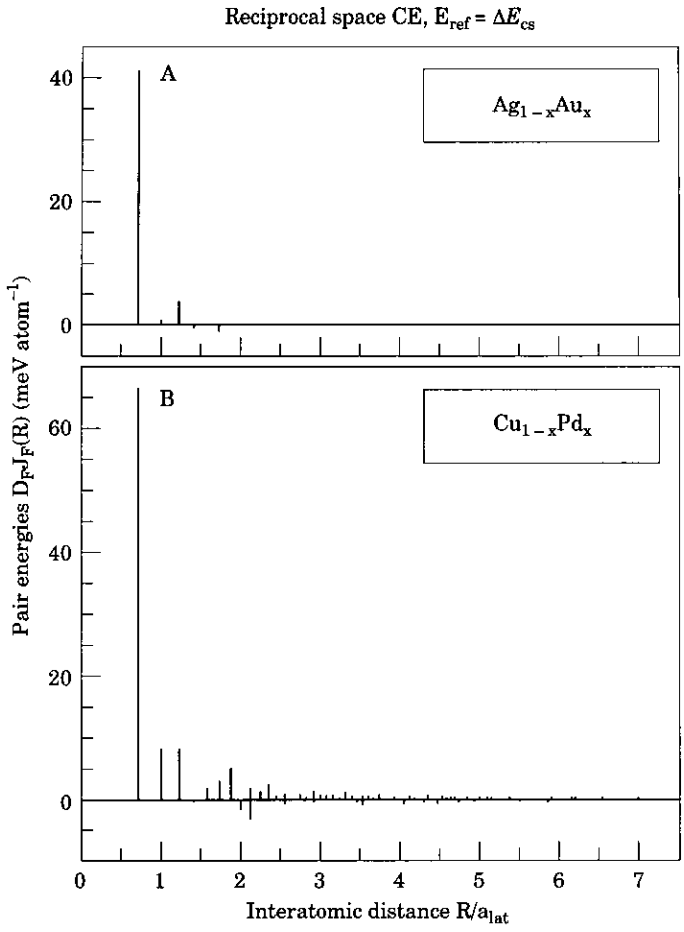


**Fig. 4.** Pair interaction energies for (A) Ag-Au and (B) Cu-Pd.

(iv) The power of the CE is illustrated in Fig. 5, depicting the predicted bulk SL formation energies $\Delta H_{SL}(pp, \hat{G})$ of SLs too complex to be calculated directly by LAPW and $\Delta H_{mix}(x)$ of the random alloy. We see that only for very short period SLs does $\Delta H_{SL} < \Delta H_{mix}$: specifically, the ordering energy of eqn (9) is negative for Ag/Au only for

$$\begin{aligned} &p<1 \text{ for } \hat{G}=(111)\\ &p<3 \text{ for } \hat{G}=(012)\\ &p<2 \text{ for } \hat{G}=(011)\\ &p<1 \text{ for } \hat{G}=(001), \end{aligned} \tag{24}$$

while for Cu/Pd the ordering energy is negative for

$$\begin{aligned} &p<1 \text{ for } \hat{G}=(111)\\ &p<3 \text{ for } \hat{G}=(012)\\ &p<2 \text{ for } \hat{G}=(011)\\ &p<1 \text{ for } \hat{G}=(001). \end{aligned} \tag{25}$$

**Table 5:** Constituent strain energy $\Delta E_{CS}^{eq}(\hat{G}, x)$ $(x = 1/2)$ and interfacial energies $I(pp, \hat{G})$ of $A_pB_p$ superlattices $(p = 50)$, the energies are in units of meV atom$^{-1}$.

| SL Orientation | [001] | [012] | [011] | [111] |
|---|---|---|---|---|
| $\Delta E_{CS}^{eq}$ (Cu/Pd) | 17.4 | 34.5 | 41.0 | 46.0 |
| $I$ (Cu/Pd) | −81.9 | −283.2 | −167.2 | −72.0 |
| $I$ (Ag/Au) | −21.7 | −65.2 | −36.1 | −14.1 |

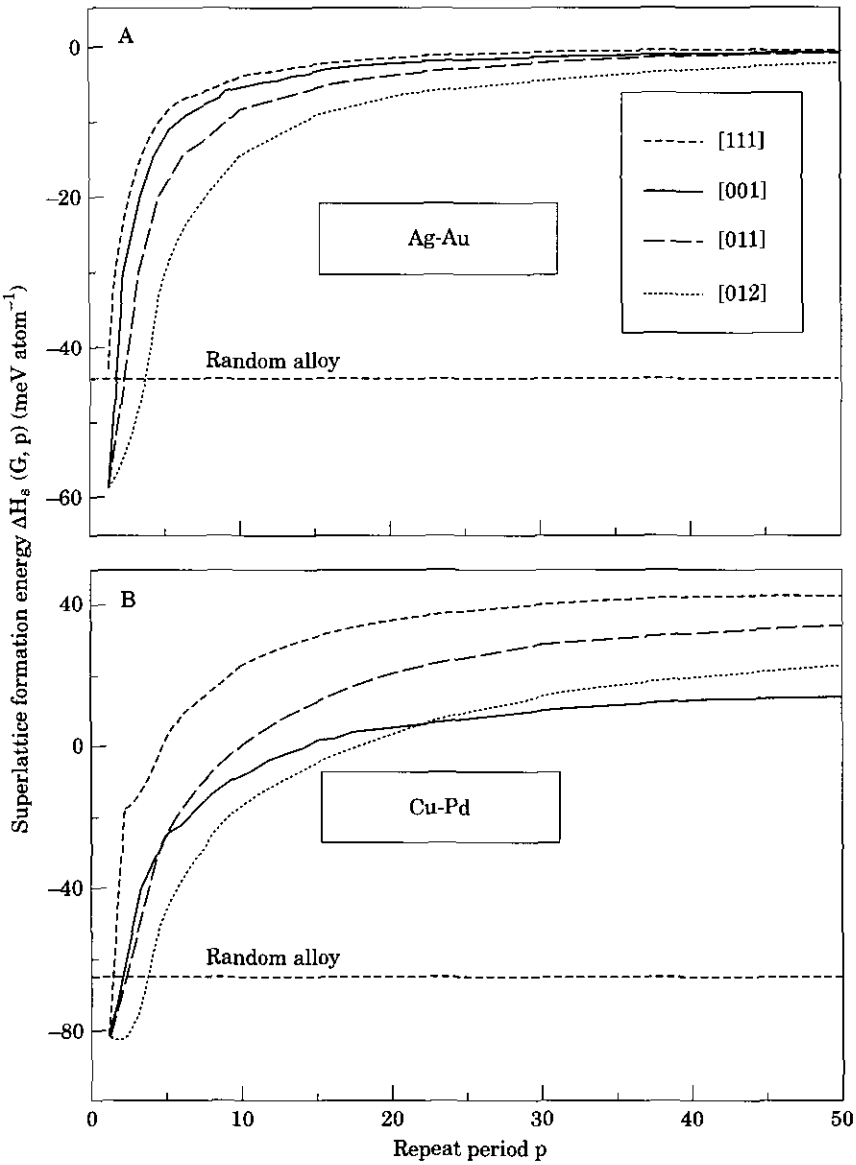


**Fig. 5.** (A) the $Ag_pAu_p$ superlattice energies as a function of repeat period $p$. As a comparison, we also show (B) the energies of the lattice-mismatched $Cu_pPd_p$ superlattices.

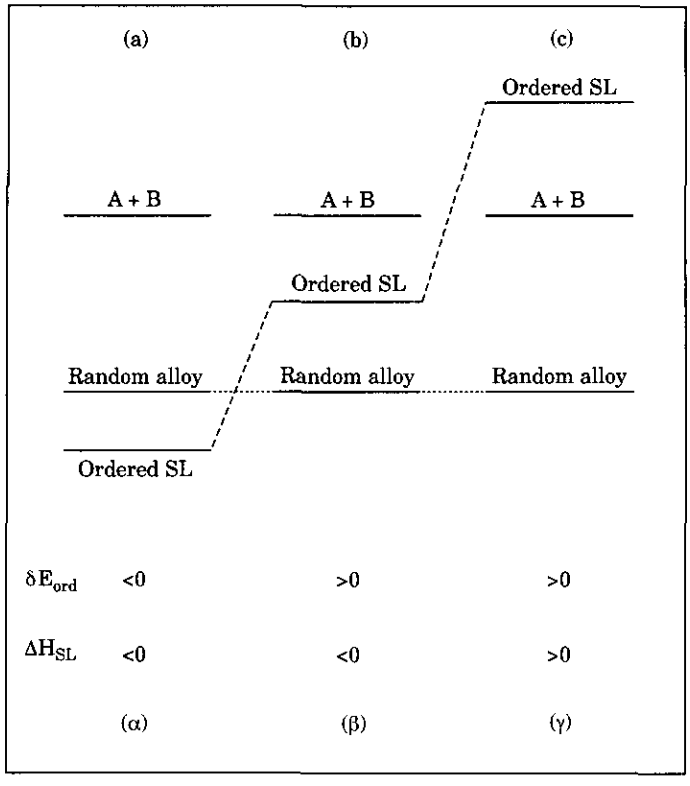


**Fig. 6.** Superlattices according to their signs of $\Delta H$ [eqn (1)] and $\delta E_{ord}$ [eqn (9)].

Thus, Ag/Au and Cu/Pd SLs are stable with respect to formation of random alloys and phase-separation only at ultra short periods of 1–3 corresponding to ordinary intermetallic compounds such as $L1_0$. This corresponds to the energy sequence $\alpha$ shown in Fig. 6(a). Above these periods we find 'region $\beta$' [Fig. 6(b)] where the SLs are stable with respect to phase-separation but unstable with respect to alloy formation. This means that some ordered structures (such as the non-superlattice $L1_2$ structure) *other* than these SLs are more stable. If, nevertheless the SL did form, it would decay into an intermixed state. Finally in 'region $\gamma$' the SLs are unstable both with respect to alloy formation *and* phase-separation. Thus, at high temperature such superlattices will disorder while at low temperature they will adopt the lowest energy ground state (if there is enough diffusion mobility); there is no temperature at which the atomic order corresponding to such SL is a thermodynamically stable structure. For Cu-Pd region $\alpha$ is for $p<3$ [eqn (25)], regions $\beta$ and $\gamma$ are for $p<5$–18 and $p>5$–18 (depending on the orientation of $\hat{G}$), respectively. For Ag-Au, region $\alpha$ is for $p<3$, region $\beta$ is for $p>3$, while region $\gamma$ does not exist.

We have addressed the stability of SLs at $T=0$ K, and we have found that the interfacial energies $I(pq, \hat{G})$ are strongly orientation and period dependent, with the [012] direction being the most stable while the [111] direction is the least stable. The free energy of the superlattice as a function of temperature can be investigated using statistical mechanics methods, e.g. with the cluster variation method (the internal energy is calculated using a cluster expansion). Entropy effects would favor disordering (alloying), thus lowering the free energy of the disordered alloy. On the other hand, the free energy of the sharply-interfaced superlttice will become less stable with respect to the 'intermixed superlattices' (disordered alloy). Hence, the atoms near the interface of a superlattice would intermix and as a result, one would expect that strong anisotropy of the interfacial energy $I(\hat{G})$ will be eliminated as temperature increases.

*Acknowledgements*—ZWL and BMK thank the support by the University Research Funds of the University of California at Davis and San Diego Supercomputer Center for computer time. AZ thanks the support by the Office of Energy Research (OER) [Division of Materials Science of the Office of Basic Sciences (BES)], U.S. Department of Energy, under the contract No. DE-AC36-83CH10093.

## References

[1] A Zunger, in *Statics and Dynamics of Alloy Phase Transformations*, eds P. E. A. Turchi and A. Gonis, NATO ASI Series B, Plenum, New York: p. 361, vol. 319 (1994).
[2] A. Zunger, in *Handbook of Crystal Growth*, ed. D. T. J. Hurll, Vol. 33, North Holland, Amsterdam: p. 998 (1994).
[3] R. G. Dandrea, J. E. Bernard, S.-H. Wei and A. Zunger, Phys. Rev. Lett., **64,** 36 (1990).
[4] D. M. Wood and A. Zunger, Phys. Rev. B, **38,** 12 756 (1988).
[5] M. Sluiter and P. E. A. Turchi, Phys. Rev. B, **46,** 2565 (1992).
[6] B. M. Klein and C. Y. Fong, in *Metallic Alloys: Experimental and Theoretical Perspectives*, eds J. S. Faulkner and R. G. Jordan, Kluwer, Dordrecht: p. 291 (1994).
[7] At very large $p$ and $q$, $\Delta H(\infty, \hat{G}) \rightarrow \Delta E_{CS}(\hat{G})$ since for Ag-Au, the lattice mismatch is very small, $\Delta E_{CS}(\hat{G})$ has a small, positive value.
[8] D. de Fontaine, *Solid State Physics*, eds H. Ehrenreich and D. Turnbull, Academic Press, New York: p. 33, vol. 47 (1994).
[9] J. M. Sanchez, F. Ducastelle and D. Gratias, Physica A, **128,** 334 (1984).
[10] D. B. Laks, L. G. Ferreira, S. Froyen and A. Zunger, Phys. Rev. B, **46,** 12 587 (1992).
[11] giro91 S. de Gironcoli, P. Giannozzi and S. Baroni, Phys. Rev. Lett., **66,** 2116 (1991).
[12] S. V. Beiden and V. G. Vaks, Phys. Lett., **163A,** 209 (1992).
[13] J. L. Martins and A. Zunger, Phys. Rev. B, **30,** 6127 (1984).
[14] Z. W. Lu, S.-H. Wei, A. Zunger, S. Frota-Pessoa and L. G. Ferreira, Phys. Rev. B, **44,** 512 (1991).
[15] M. E. Fisher and W. Selke, Phys. Rev. Lett., **44,** 1502 (1980).
[16] A. Zunger, S.-H. Wei, L. G. Ferreira and J. E. Bernard, Phys. Rev. Lett., **65,** 352 (1990).
[17] S.-H. Wei, L. G. Ferreira, J. E. Bernard and A. Zunger, Phys. Rev. B, **42,** 9622 (1990).
[18] Z. W. Lu, S.-H. Wei and A. Zunger, Phys. Rev. B, **44,** 10 470 (1991).
[19] Z. W. Lu, S.-H. Wei and A. Zunger, Phys. Rev. B, **44,** 3387 (1991).
[20] Z. W. Lu, S.-H. Wei and A. Zunger, Phys. Rev. B, **45,** 10 314 (1992).
[21] Here, we use a nearly identical set of input structures for Cu-Pd and Ag-Au. In our previous work for Ag-Au (Z. W. Lu, B. M. Klein and A Zunger. *Modelling and Simulation in Materials Science and Engineering* p. 753, vol. 3 (1995)), we have used a slightly larger set of input structures (17 instead of 16) and a larger number of interactions (12 instead of 10 here). We find here that the interaction are very similar to the present ones to within 0.9 meV atom$^{-1}$.
[22] O. K. Andersen, Phys. Rev. B, **12,** 3060 (1975).
[23] E. Wimmer, H. Krakauer, M. Weinert and A. J. Freeman, Phys. Rev. B, **24,** 864 (1981).
[24] D. R. Hamann, Phys Rev. Lett., **42,** 662 (1979).
[25] S.-H. Wei and H. Krakauer, Phys. Rev. Lett., **55,** 1200 (1985).
[26] S.-H. Wei, H. Krakauer and M. Weinert, Phys. Rev. B, **32,** 7792 (1985).
[27] D. J. Singh, *Planewaves, Pseudopotentials, and the LAPW Method.* Kluwer, Boston: (1994).
[28] P. Hohenberg and W. Kohn, Phys. Rev. B, **136,** 864 (1964).
[29] W. Kohn and L. J. Sham, Phys. Rev. A, **140,** 1133 (1965).
[30] D. M. Ceperley and B. J. Alder, Phys. Rev. Lett., **45,** 566 (1980).
[31] J. P. Perdew and A. Zunger, Phys. Rev. B, **23,** 5048 (1981).
[32] S. Froyen, Phys. Rev. B, **39,** 3168 (1989).
[33] H. J. Monkhorst and J. D. Pack, Phys. Rev. B, **13,** 5188 (1976).
[34] E. Wigner, Phys. Rev., **46,** 1002 (1934).